Direct laser written aperiodic photonic volume elements for complex light shaping with high efficiency: inverse design and fabrication: supplemental document

Nicolas Barré[1,2,4], Ravi Shivaraman[3], Simon Moser[1], Patrick Salter[3], Michael Schmidt[2,4], Martin J. Booth[3,4], Alexander Jesacher[1,4,*]

[1]Institute of Biomedical Physics, Medical University of Innsbruck, Müllerstraße 44, 6020 Innsbruck, AT
[2]Institute of Photonic Technologies, Friedrich-Alexander-University Erlangen-Nürnberg, Konrad-Zuse-Straße 3/5, Erlangen 91052, DE
[3]Department of Engineering Science, University of Oxford, Parks Road, Oxford OX1 3PJ, UK
[4]Erlangen Graduate School in Advanced Optical Technologies (SAOT), Friedrich-Alexander-University Erlangen-Nürnberg, Paul-Gordan-Straße 6, 91052 Erlangen, DE

S1. APVE characterization

The APVEs are characterized with the home-built imaging system shown in Fig. S1. The setup allows one to focus fiber coupled laser beams of three different wavelengths (Toptica ibeam smart @640 nm, Lasos LGK7786P @543 nm, Thorlabs laser diode PL450B @455 nm) onto the input facet of a APVE, which rests on a manual 3D micro stage. The waists of the laser foci can be controlled by choosing appropriate focal lengths for the lenses 4, 5 and 6. A motorized tip/tilt mirror is imaged onto the APVE input facet using a Keplerian telescope. This allows one to precisely control the laser's AOI. The output facet is imaged using a microscope objective lens (Olympus UPlanFL, 10x, 0.3 NA), whose exit pupil is imaged onto an iris with tunable aperture. This iris was used to restrict the imaging NA to 0.05 when characterizing the mode sorter. Finally, an image of the end facet is formed at the sensor of a CCD camera (Basler puA1600-60uA). Optionally, a Bertrand lens can be flipped in for imaging the objective's exit pupil, which is used to calibrate the laser AOIs. The setup further comprises a Mach-Zehnder interferometer for measuring complex field distributions at the output of the mode sorter APVE using off-axis interferometry.

Interferometry

To characterize the quality of the mode sorter, it is required to measure the complex light field at the output facet of the APVE. This is done using off-axis interferometry using a Mach-Zehnder interferometer. The reference wave is tilted, such that the interference fringes have period of about 3 pixels as shown in Fig. S2 (a). The intensity image is Fast Fourier transformed (FFT), followed by cropping a 60×60 pixel region around one sideband as shown in Fig. S2 (b). The complex field is then obtained by taking an inverse FFT of the cropped sideband. However, at this stage it will most likely show only a poor overlap with any HG mode. This is because of several factors: Firstly, the field is usually not perfectly centered on the pixel grid and there could be a small geometric rotation in the experimental images. Secondly, the presence of a global phase tilt and defocus is likewise reducing the overlap integral. Finally, the waist of the measured mode could be slightly different compared to the simulation.

To solve these issues, we employed a Nelder Mead optimizer (Julia programming language, toolbox: Optim.jl) to find those seven parameters (x-shift, y-shift, rotation, x-tilt, y-tilt, defocus, waist) which maximize the overlap integral between light field obtained at 0° AOI and the matching target mode $\mathrm{HG}_{1,1}$. The optimal parameters identified for mode $\mathrm{HG}_{1,1}$ have also been used to

process the five remaining experimentally recorded mode fields. We emphasize that we have *not* optimized the overlap integral of each mode individually, as our intention is to present numbers that can be achieved in a practical experiment.

S2. Additional information on the colour multiplexer

Figure S3 shows output intensities of the colour smiley APVE, taken with the monochromator light source at wavelengths varied from 420 nm to 680 nm in steps of 10 nm. For APVE characterization, the light form the monochromator's arc lamp was focused into a light guide of 1 mm diameter. About 1 cm from light guide's output we placed a 100 µm pinhole to further increase the spatial coherence. This pinhole was then imaged with a slight demagnification (telescope with 200 mm and 150 mm lenses) onto the motorized tip/tilt mirror shown in Fig. S1, such that the monochromator light at the input facet of the APVEs took the form of a Gaussian with $w_0 \approx 30$ µm.

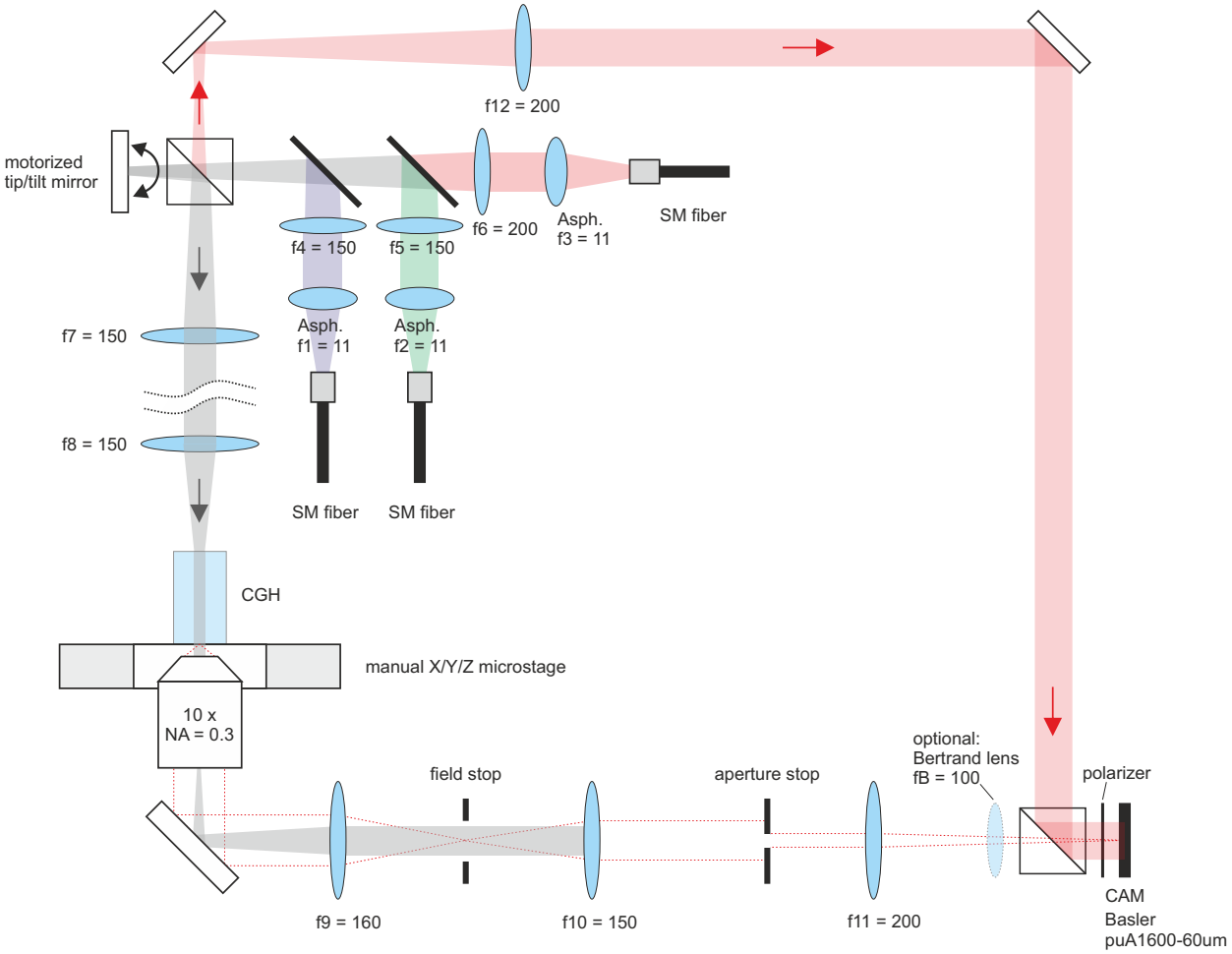

Fig. S1 Optical setup for characterizing APVEs. A motorized tip/tilt mirror is imaged onto the input facet of the APVE, which rests on a manual x/y microstage. The APVE can be simultaneously exposed to three laser beams (red/green/blue) or optionally to light form the monochromator (not shown). The APVE output facet is imaged from below, where the imaging NA can be controlled by an aperture stop. The setup further features a Mach-Zehnder interferometer for characterizing the mode sorter APVE.

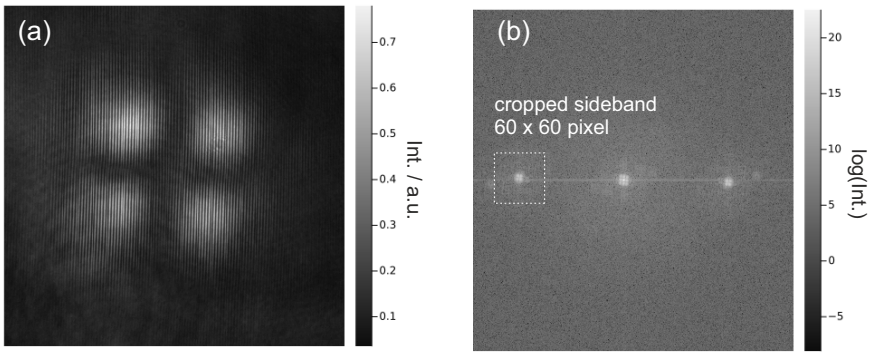

Fig. S2 Interferometry to characterize the light field shaped by the mode sorter. Left: Raw interferogram captured by the camera; Right: Its logarithmic power spectrum. One sideband is cropped for further processing.

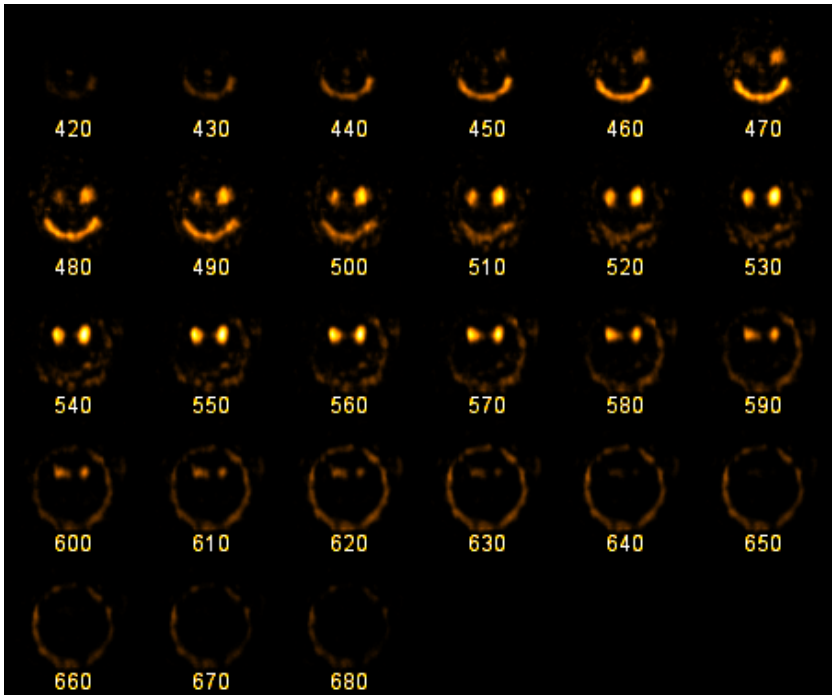

Fig. S3 Wavelength dependent output intensities of the colour smiley APVE. The illumination light was provided by a tunable monochromator. The numbers below the images denote the respective wavelength in nm.

S3. Additional information on the mode sorter

Figure S4 presents a table of 30×30 intensity images, which appear at the output facet of the mode sorter when the AOI of the input beam is altered in increments of 0.11 degrees (in air). One can clearly identify six angular regions where the output pattern resembles a particular HG mode. Figure S5 shows the measured transmission T of the mode sorter as a function of the laser AOI. One can clearly define six local maxima, whose respective peak values match the numbers in table 5 of the main document. Finally, Fig. S6 visualizes the measured angular dependence of all six efficiency values $\eta_{i,j}$ as defined by Eq. 3 of the main document.

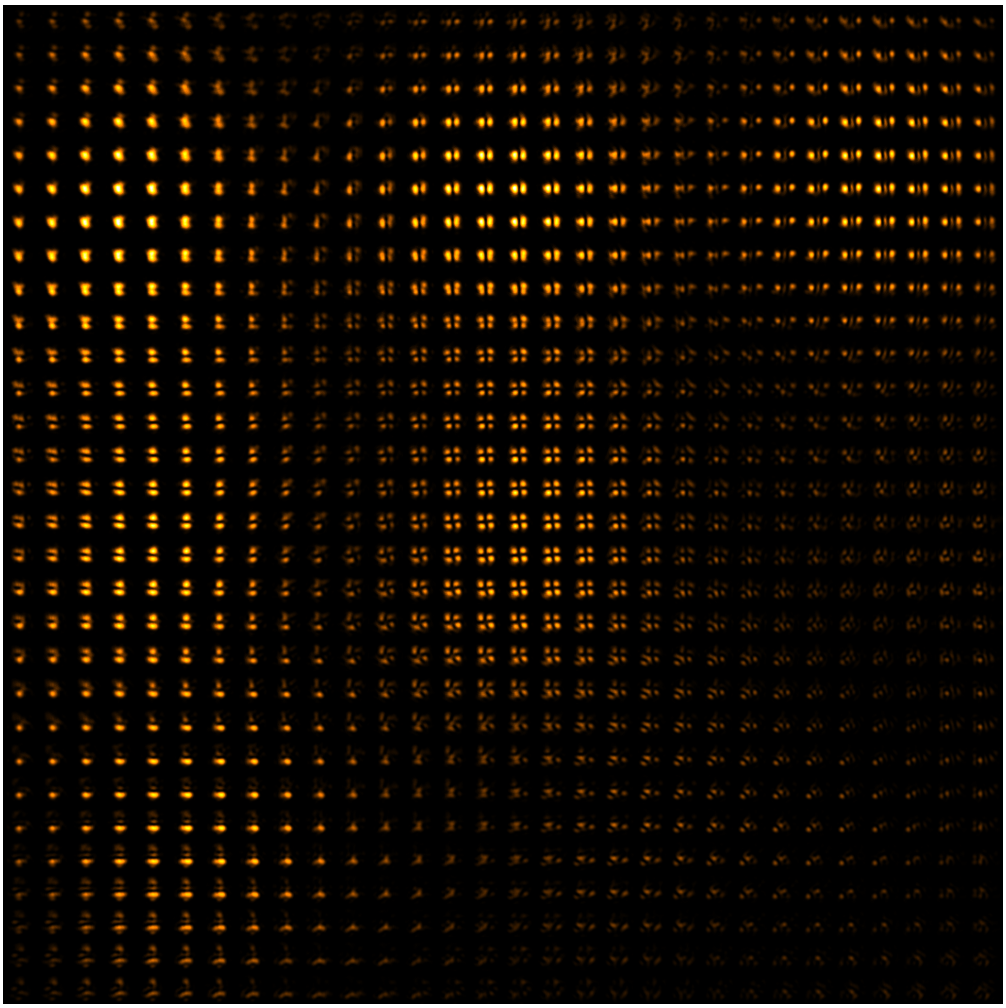

Fig. S4 Angular dependent readouts of the mode sorter APVE. The figure shows 30×30 images, each one showing the intensity at the APVE output facet for a different incidence angle of the readout beam. The angular increment from one image to the next is 0.11 degrees. The image showing the $HG_{1,1}$ mode in the center corresponds to a readout angle of zero.

S4. Manufacturing of APVEs

The APVEs were manufactured using the direct laser writing technique [49]. The beam from an ultrafast laser (Light Conversion, Pharos SP 6W) emitting pulses with 170 fs duration, at a repetition rate of 1 MHz and wavelength 515 nm was expanded and directed toward a phase-only liquid crystal spatial light modulator (SLM) (Hamamatsu X10468). The SLM was imaged in 4f configuration onto the pupil plane of a microscope objective (Zeiss 20× 0.5NA). The beam was thus focused into the glass sample (Corning EAGLE 2000) to fabricate the APVE voxels. The sample was mounted on a precision 3D translation stage (Aerotech ABL10100 (x-z), ANT-95V (y)) and moved through the laser focus at a speed of 2 mm/s in the z direction, as defined in Figure 1 (a) of the main document. The PSO function was used to gate the laser according to the design specification and fabricate voxels at the desired position. The laser pulse energy was 37 nJ and the polarisation was linear along the translation direction. We note that this pulse energy is significantly lower than that which would typically be used to write single mode optical waveguides

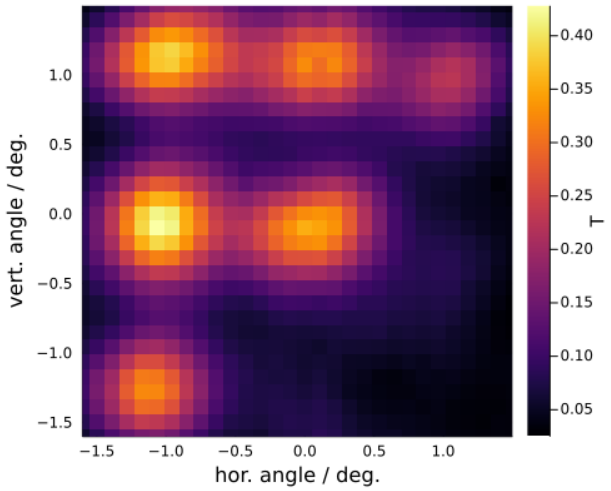

Fig. S5 Angular dependence of the transmission T of the mode sorter. The figure shows the measured power fraction of the input beam arriving the camera sensor.

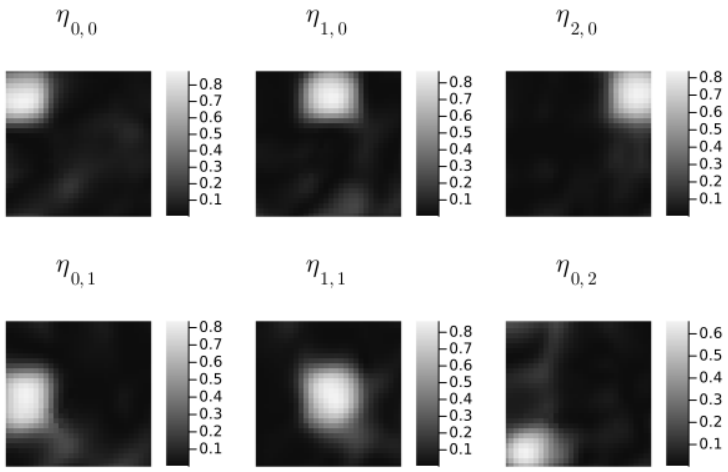

Fig. S6 Angular dependence of the experimental efficiency values $\eta_{i,j}$ of the mode sorter.

in such a system. As the sample was moved in the y direction to build up different layers of the APVE, the phase pattern displayed on the SLM was updated to compensate for depth-induced spherical aberration arising from refraction at the sample surface [50].

S5. Design algorithm

In the following, we present an algorithm that allows to design voxel-based APVEs for the conversion of N mutually incoherent transverse input modes $\{u_n\}_{1\leq n\leq N}$ to N target modes $\{v_n\}_{1\leq n\leq N}$, with a one-to-one mapping. In general, any pair of modes (u_n, v_n) has its own wavelength λ_n. We consider the design of a finite extent sample in a rectangular coordinate system (O, x, y, z), z being the direction of propagation. We denote z_{in} the transverse plane where the input modes $\{u_n\}$ are defined, and z_{out} the destination plane where the target modes $\{v_n\}$ are defined. The bulk refractive index of the sample at wavelength λ_n is denoted n_n. In terms of fabrication capabilities, we assume that we have access to a diversity of transverse voxel distributions that we are

able to write in the glass sample at any 3D location, and that the length of any voxel (i.e., the z dimension) can be freely chosen. One example of a voxel cross section is given in Figure 1 (b) of the main document, but many more are possible by varying the writing parameters such as the pulse energy or the aberration compensation term. Let us note D the number of different transverse voxel distributions $\{\Delta\mathrm{RI}_d\}_{1\leq d\leq D}$ which we consider to use for the inverse design. These transverse distributions are relative refractive index changes compared to the bulk refractive index, and are possibly wavelength dependent. By convention, we also define $\Delta\mathrm{RI}_0$ to refer to a null refractive index modification. In order to make the inverse design much simpler, the sample volume is virtually split into sub-volumes v_{ijk}, $1 \leq i \leq I$, $1 \leq j \leq J$, $1 \leq k \leq K$, acting as placeholders for the elementary voxel distributions $\{\Delta\mathrm{RI}_d^{ijk}\}$. These sub-volumes extensions in 3 dimensions are denoted $\mathrm{D}x$, $\mathrm{D}y$ and $\mathrm{D}z$. Thus, the possible lengths of the waveguides used for the design can only be integer multiples of the elementary length $\mathrm{D}z$. In our designs, this elementary length is typically $\mathrm{D}z = 10\,\mu\mathrm{m}$. For the simulation to be numerically accurate, the sampling resolution in 3 dimensions $\mathrm{d}x$, $\mathrm{d}y$ and $\mathrm{d}z$ must be much better, typically $\mathrm{d}x = \mathrm{d}y = 0.25\,\mu\mathrm{m}$ and $\mathrm{d}z = 0.5\,\mu\mathrm{m}$.

Forward model

The propagation of the input modes $\{u_n\}$ from the plane z_{in} to the plane z_{out} relies on the split-step Fourier beam propagation method (BPM), with spatial resolutions $\mathrm{d}x$, $\mathrm{d}y$ and $\mathrm{d}z$. The input modes cross the sub-volumes v_{ijk} layer by layer, for k varying from 1 to K. Each sub-volume v_{ijk} may contain (or not) one of the possible transverse distributions $\{\Delta\mathrm{RI}_d^{ijk}\}$, depending on the choice that was made in a previous iteration by the selection algorithm that we present next. During this forward propagation, the transverse distributions $\{u_n\}$ are saved before crossing each sub-volume v_{ijk}, and we note them $\{u_n^{ijk}\}$ for future reference. We also note $\{z_k\}$ the common transverse planes where these distributions are saved.

According to the BPM, for a given input mode u_n, crossing each layer of thickness $\mathrm{d}z$ is modeled as a small propagation of length $\mathrm{d}z$ through an homogeneous medium of refractive index n_n, followed by the multiplication of a local phase φ_{ijk} depending on the activated region:

$$\varphi_{ijk}(\lambda_n) = \exp\left(i\frac{2\pi}{\lambda_n}\Delta\mathrm{RI}_d^{ijk}(\lambda_n)\mathrm{d}z\right),\ 0 \leq d \leq D. \tag{S1}$$

Error metric

Our inverse design relies on a multi-objective minimization based on the squared l_2 distance between the input and target modes:

$$O_{min} = \min\left\{\sum_{n=1}^{N}\|u_n - v_n\|_2^2\right\} = \min\left\{\sum_{n=1}^{N}\int_{z_{out}}|u_n - v_n|^2\right\}. \tag{S2}$$

We can expand the squared modulus as $|u_n - v_n|^2 = |u_n|^2 + |v_n|^2 - 2\Re(v_n^* u_n)$, which allows to turn the minimization problem (Eq. S2) into the following maximization problem in the case of a lossless design ($\|\|_2^2$ of u_n and v_n is conserved):

$$O_{max} = \max_{\{\Delta\mathrm{RI}_d^{ijk}\}}\left\{\sum_{n=1}^{N}\int_{z_{out}}\Re\left(v_n^* u_n\right)\right\}. \tag{S3}$$

Equation S3 consists only of overlap integrals that are conserved during propagation (or backpropagation) through a lossless optical system, thus allowing for an iterative propagation algorithm (IPA) [51], where the same criterion O_{max} is iteratively maximized in each plane z_k (in a reverse fashion).

Voxel distribution selection algorithm

We assume that we know the transverse distributions $\{v_n^{ijk+1}\}$ corresponding to the local distributions of the target modes $\{v_n\}$ in the plane z_{k+1} just after the sub-volumes $\{v_{ijk}\}$, and the transverse distributions $\{u_n^{ijk}\}$ of the input modes $\{u_n\}$ stored just before the same sub-volumes. The selection of the refractive index distribution ΔRI_d^{ijk} relies on the maximization of the local multi-objective criterion

$$O_{max}^{ijk} = \max_d \left\{ \sum_{n=1}^{N} \int_{z_{k+1}} \Re\left((v_n^{ijk+1})^* u_n^{ijk+1}(d) \right) \right\}, \tag{S4}$$

where $u_n^{ijk+1}(d)$ denotes the local input modes distribution that have been propagated from plane z_k, where they were stored during the forward pass, to plane z_{k+1} through a local refractive index distribution ΔRI_d^{ijk}. In order to find d maximizing O_{max}^{ijk}, all the distributions $\{\Delta\text{RI}_d^{ijk}\}$ need to be tried for each sub-volume v_{ijk} (k fixed).

Once the $\{\Delta\text{RI}_d^{ijk}\}$ distributions have been selected for a given k, the target modes $\{v_n^{ijk+1}\}$ are backpropagated to the plane z_k, and the same procedure is repeated iteratively until the selection of the $\{\Delta\text{RI}_d^{ij1}\}$.

Iterative propagation algorithm

We summarize the different steps of the optimization procedure below:

1. Propagate the input modes $\{u_n\}$ from their definition plane $z_{in} = z_1$ to the destination plane $z_{out} = z_{K+1}$ using BPM, taking into account the current waveguide selection in each sub-volume v_{ijk} ($1 \leq k \leq K$). At the beginning of the first iteration, all $\{v_{ijk}\}$ contain a null refractive index distribution (ΔRI_0). During propagation, store the local field distributions $\{u_n^{ijk}\}$ at planes $\{z_k\}$.

2. Compute the final overlap criterion (Eq. S3) for monitoring the convergence of the algorithm. If the convergence is satisfactory or stagnant, then exit the optimization procedure and consider the current waveguide selection as the optimal design.

3. Iteratively backpropagate the target modes $\{v_n\}$ from plane $z_{out} = z_{K+1}$ to plane $z_{in} = z_1$, while proceeding to a new voxel selection in each sub-volume v_{ijk} according to the criterion in Eq. S4. For a given k, this criterion leads to the best voxel selection in each sub-volume, after which the modes $\{v_n\}$ in plane z_{k+1} can be backpropagated to plane z_k, and this iteratively until $k = 1$.

4. Repeat the procedure from step 1.